Gap solitons in quasiperiodic optical lattices

Hidetsugu Sakaguchi[1] and Boris A. Malomed[2]
[1]*Department of Applied Science for Electronics and Materials, Interdisciplinary Graduate School of Engineering Sciences, Kyushu University, Kasuga, Fukuoka 816-8580, Japan*
[2]*Department of Interdisciplinary Studies, Faculty of Engineering, Tel Aviv University, Tel Aviv 69978, Israel*
(Received 5 March 2006; revised manuscript received 25 May 2006; published 8 August 2006)

Families of solitons in one- and two-dimensional (1D and 2D) Gross-Pitaevskii equations with the repulsive nonlinearity and a potential of the quasicrystallic type are constructed (in the 2D case, the potential corresponds to a fivefold optical lattice). Stable 1D solitons in the weak potential are explicitly found in three band gaps. These solitons are mobile, and they collide elastically. Many species of tightly bound 1D solitons are found in the strong potential, both stable and unstable (unstable ones transform themselves into asymmetric breathers). In the 2D model, families of both fundamental and vortical solitons are found and are shown to be stable.

DOI: 10.1103/PhysRevE.74.026601 PACS number(s): 42.65.Tg, 03.75.Lm, 61.44.Br, 42.70.Qs

I. INTRODUCTION

Solitons in Bose-Einstein condensates (BECs) are currently a subject of intensive theoretical and experimental studies. Solitons supported by weak attractive interactions between atoms were created in the condensate of ^{7}Li trapped in strongly elongated [nearly one-dimensional (1D)] traps [1] (although the actual shape of the solitons was actually nearly three-dimensional, rather than nearly 1D; the latter feature was observed in a salient form in the recent experiment [2], where solitons were created as a residual pattern after dynamical collapse took place in the ^{85}Rb condensate). The stability of the solitons, with a given number of atoms, against collapse is secured, in these settings, by a combination of the trap's geometry and small absolute value of the negative scattering length characterizing the attraction between atoms ($\sim$0.1 nm in the case of ^{7}Li, but up to $\sim$2 nm in the condensate of ^{85}Rb). A very accurate description of the solitons is provided by the mean-field approximation based on the Gross-Pitaevskii equation (GPE) [3].

Positive scattering length, which corresponds to repulsive interactions, is more generic in BEC (in the above-mentioned experiments, the negative scattering length was actually artificially induced by means of the Feshbach resonance, both in ^{7}Li and ^{85}Rb). In a repulsive condensate, *gap solitons* (GSs) may be created as a result of the interplay of the self-defocusing nonlinearity and periodic potential induced by an optical lattice (OL, i.e., an interference pattern created by counterpropagating laser beams illuminating the condensate) [4,5]. GSs emerge in *band gaps* of the system's linear spectrum, since the combination of a *negative* effective mass, appearing in a part of the bands adjacent to the gaps, with the repulsive interaction is exactly what is needed to create a soliton. Theoretical models for GSs in BEC were reviewed in Ref. [6], and rigorous stability analysis for them in the 1D case was developed in Ref. [7]. Creation of a GS in the experiment was reported in Ref. [8], in ^{87}Rb condensate placed in a quasi-1D trap supplemented by a longitudinal OL; the soliton contained a few hundred atoms. In a subsequent experiment, large-size confined states with much larger numbers of atoms were discovered in a stronger OL [9]; an explanation of this observation was recently proposed [10], which, essentially, treats the extended state as a segment of a nonlinear Bloch wave, bounded by two fronts (domain walls) that are sustained by the strong OL (a similar wall between filled and empty domains was predicted in BEC with self-attraction in Ref. [11]).

Stable GSs were also predicted in 2D and 3D settings [5], including 2D solitons with embedded vorticity [12,13]. In nonlinear optics, similar 2D spatial solitons [14] and 2D localized vortices [15] were predicted in photonic crystals and photonic-crystal fibers, as well as in periodic photonic lattices induced by perpendicular laser beams in photorefractive materials [16]. In media of the latter type, both fundamental [17] and vortical 2D solitons have been created in the experiment [18]. A difference from the self-repulsive BEC is the self-focusing character of the nonlinearity in nonlinear optics (which is cubic in photonic crystals and saturating in photorefractive media); for this reason, the optical solitons usually belong to the semi-infinite band gap, where the effective mass is always positive (although vortex solitons in a finite gap were also created in a photorefractive medium [19]).

The GPE with self-attraction and periodic (optical-lattice) potential gives rise to 2D solitons and vortices [20] similar to those found in the above-mentioned optical models. Moreover, it has been recently demonstrated that both the GPE with the self-focusing cubic term and OL potential, and its counterpart with the saturable nonlinearity, that pertains to photorefractives, give rise to stable higher-order localized vortices (which are built as rings of unitary vortices) and *supervortices* (similar rings with global vorticity imprinted onto them) [21].

Quasiperiodic OLs can be easily created too: in the 1D case, as a superposition of two sublattices with incommensurate periods, and in the 2D case, as a combination of $N=5$ or $N\geqslant 7$ quasi-1D sublattices with wave vectors $\mathbf{k}^{(n)}$ of equal lengths, which make equal angles $2\pi/N$ between themselves. In particular, the 2D lattice with $N=5$ is known as the *Penrose tiling* (PT). The band-gap spectrum of 2D photonic crystals of the PT type has been studied in detail [22], with a conclusion that true (omnidirectional) band gaps may be supported by the PT.

The use of quasiperiodic lattices, in one and two dimensions alike, offers new degrees of freedom that allow one to *engineer* desirable band gaps in the spectrum and, in this

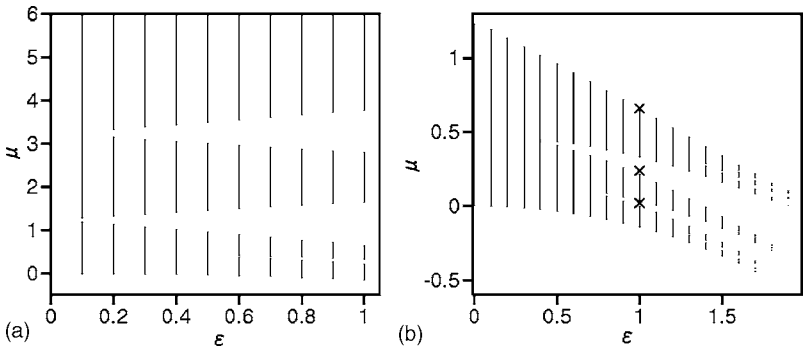

FIG. 1. A part of the band-gap structure in the linear version of Eq. (1). Crosses in (b) indicate values of μ for three GSs shown in Fig. 2.

way, *design* soliton families in nonlinear media. Several theoretical works sought for solitons in models combining quasiperiodic lattice potentials and cubic *self-focusing*. In an early work [23], solitons were not found in a 1D quasiperiodic model; however, they were later discovered in a "deterministic aperiodic" discrete nonlinear Schrödinger (NLS) equation, which may be regarded as a limit case of the 1D model with a very strong quasiperiodic potential [24]. Localized and delocalized solutions were also studied in the 1D model with a superlattice (i.e., an ordinary OL subjected to an additional modulation, which is different from a quasicrystal) [25]. Recently, 2D solitons (with zero vorticity) were numerically constructed in a model of a photonic crystal made of a self-focusing material, with $N=12$, in terms of the above definition [26].

The objective of this work is to find GSs supported by the interplay of the cubic *repulsive* nonlinearity and quasiperiodic lattice potentials. We will report systematic results for fundamental solitons in the 1D and 2D models (the latter one will be elaborated for the PT lattice). In the 1D case, loosely bound GSs in the weak lattice are mobile. Tightly bound GSs in the strong lattice are found in many modifications, some stable and some not. Stable vortex solitons in the PT potential will be demonstrated too.

II. ONE-DIMENSIONAL SOLITONS

In the mean-field approximation, the evolution of the single-atom function ϕ obeys the GPE with the repulsive nonlinear term and quasiperiodic potential $U(x)$. In the normalized form, the equation is

$$i\frac{\partial \phi}{\partial t} = -\frac{1}{2}\frac{\partial^2 \phi}{\partial x^2} + |\phi|^2\phi + U(x)\phi. \tag{1}$$

As said above, the 1D potential is a combination of two incommensurate spatial harmonics with equal amplitudes ε,

$$U(x) = -\varepsilon\{\cos[\pi(x - L/2)] + \cos[q\pi(x - L/2)]\}, \tag{2}$$

where $x=L/2$ is the central point of a large ($L \gg 1$) trapping domain, $0<x<L$, the period of the first sublattice is normalized to be 2, and q is an irrational number. Below, we display results for $q=(\sqrt{5}+1)/2 \approx 1.62$.

As is known, an exact band-gap spectrum of the linear Schrödinger equation with a quasiperiodic potential is fractal. Without the aim to display the spectrum in full detail, in Fig. 1 we show the part that is relevant to the quest for gap solitons. Bands of values of chemical potential μ corresponding to families of quasi-Bloch states,

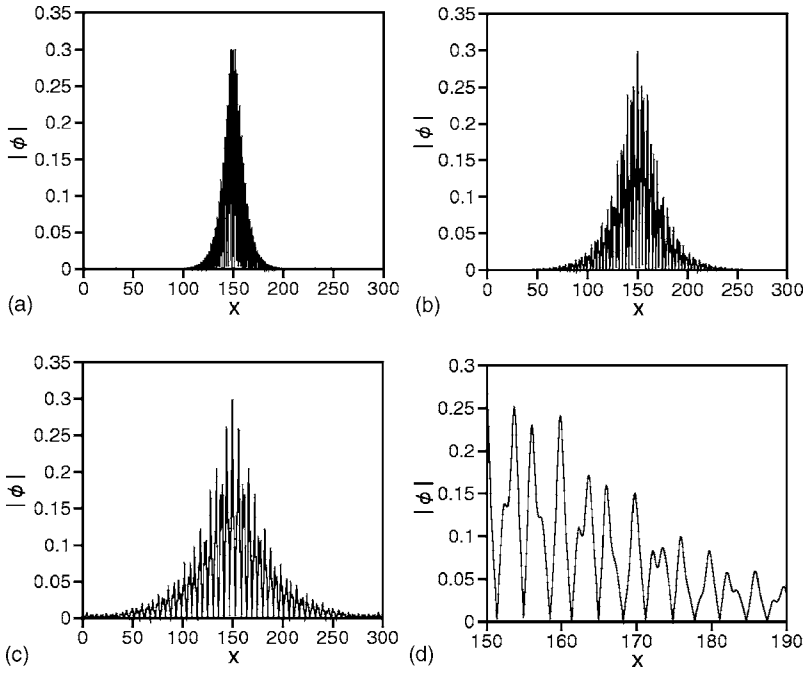

FIG. 2. Examples of stable gap solitons in the 1D model for $\varepsilon=1$, with the chemical potential and norm $\mu=0.658$, $N=0.104$ (a), $\mu=0.237$, $N=0.763$ (b), and $\mu=0.0196$, $N=0.935$ (c). Panel (d) is a blow-up of (b) in the region of $150<x<190$.

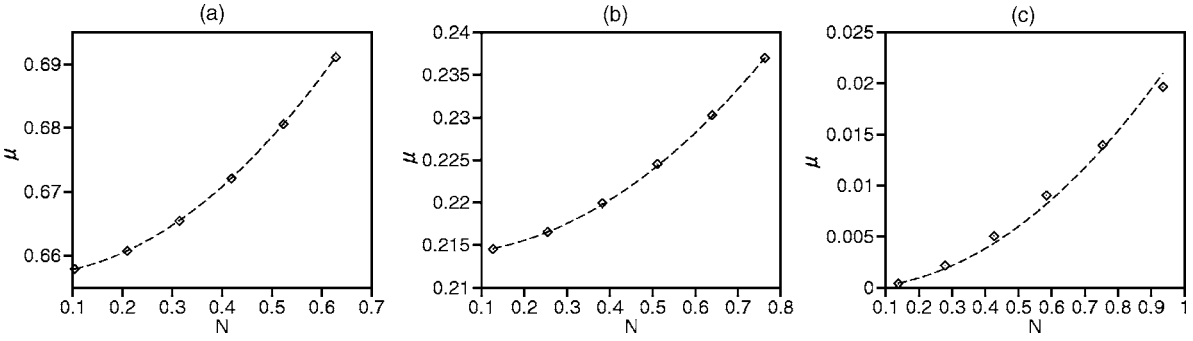

FIG. 3. The chemical potential vs norm for gap-soliton families in three lowest finite band gaps (a,b,c) of the 1D model with $\varepsilon=1$. The dashed curves are added as guides to the eye.

$$\phi(x,t) = e^{-i\mu t}\chi(x), \tag{3}$$

are covered by vertical segments at fixed values of OL strength ε. In Fig. 1(a), one can discern four finite gaps (discontinuities between the bands, the lowest gap being extremely narrow) and the underlying semi-infinite gap (one extending to $\mu\to-\infty$). A result of the standard perturbation theory is that these gaps start (at $\varepsilon=0$) at $\mu=\pi^2/2$ and $\mu=(\pi q)^2/2$. Figure 1(b) details the results in a narrower range of μ but for an extended interval of ε. One can observe, in particular, that the lowest band in Fig. 1(a) splits into two bands at $\varepsilon=0.8$ and three bands at $\varepsilon=1$ in Fig. 1(b). With the increase of ε, additional band gaps open up on a finer scale (accurate computation of the spectrum becomes rather difficult for $\varepsilon>2$).

As the effective mass is negative near the top of (quasi-)Bloch bands, GSs are expected to exist in adjacent lower parts of the gaps. Assuming real $\chi(x)$ and varying μ in Eq. (3), we numerically searched for a family of solutions of the corresponding stationary version of Eq. (1), $\chi''/2=\chi^3+U(x)\chi-\mu\chi$, satisfying boundary conditions $\chi(x=L/2)=A$, $\chi'(x=L/2)=\chi(x=L)=0$. Figure 2 displays three typical examples of GSs with equal amplitudes, $\chi(x=L/2)=A=0.3$, that were found in three finite band gaps for $\varepsilon=1$ at values of μ marked by crosses in Fig. 1(b) [as usual (in the GPE with self-repulsion), no solitons are found in the semi-infinite gap]. A blow-up of the GS in Fig. 2(b) is shown in Fig. 2(d), to demonstrate that, while the envelope of the solution is that of a solitary wave, the carrier wave function is nearly quasiperiodic.

Families of the GS solutions are characterized by the dependence of μ on the soliton's norm, $N=\int_{-\infty}^{+\infty}\chi^2(x)dx$. For GS families in the three lowest finite band gaps, whose examples were displayed in Fig. 2, the $N(\mu)$ dependences are plotted in Fig. 3. Naturally, $N\to 0$ corresponds to μ approaching the border of the quasi-Bloch band located under the respective gap.

The numerically found solution branches do not cover the range of μ corresponding to the entire band gap in each case. However, the effective termination of the branches inside the gaps seems to be a numerical problem, rather than a true feature of the model: it is difficult to secure convergence of the numerical solutions for very large values of N.

Stability analysis of the GSs was performed by means of direct simulations, using the split-step method with 4096 Fourier modes. This way, it was concluded that all the three families displayed in Fig. 3 are completely stable.

GSs obtained above can be readily set in motion in the same way as was done in Ref. [27], i.e., multiplying a stationary solution by $\exp(ikx)$, with k not too large. Examples are displayed in Fig. 4, where the "shove factor" and the resulting average velocity of the moving soliton are $k=0.03$, $v=-0.104$ (a); $k=0.015$, $v=-0.117$ (b); and $k=0.005$, $v=-0.03$ (c). Accordingly, the effective GS mass $M\equiv k/v$ is −0.288 (a), −0.128 (b), and −0.17 (c). The mass is negative, as it should be for GSs [27]. On the other hand, moving solitons feature conspicuous radiation losses if they are set in motion by shove k exceeding a certain critical value, which is $k_{\rm cr}\approx 0.05$, 0.017, and 0.008 for the solitons from Figs. 2(a)–2(c), respectively, although the transition to the lossy motion regime is not very sharp.

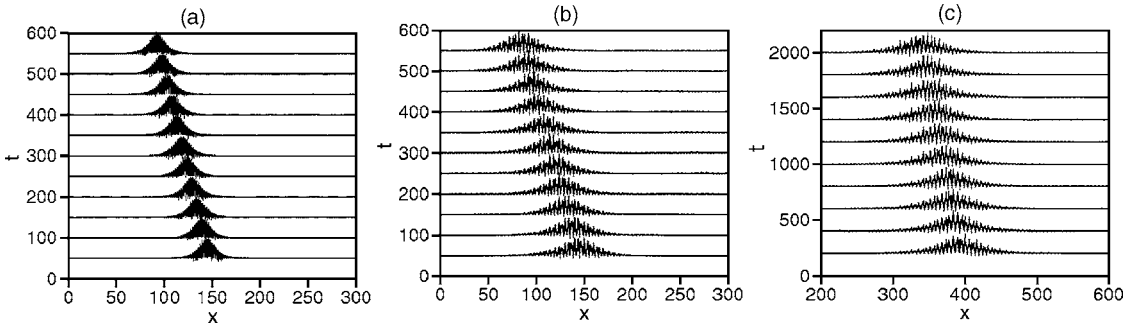

FIG. 4. Examples of stable moving gap solitons in three finite band gaps (a,b,c) of the 1D model.

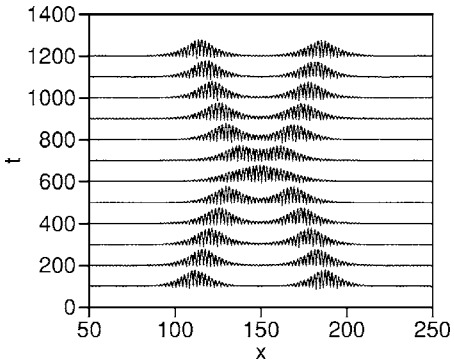

FIG. 5. Head-on collision of two gap solitons, which are obtained from ones displayed in Fig. 2(a) by shoving them with $\exp(\pm ikx)$, $k=0.02$.

Following the approach based on the separation of rapidly and slowly varying functions, one can approximate GS solutions by

$$\phi(x,t) = e^{-i\mu t}\varphi_\mu(x)\Phi(x,t), \tag{4}$$

where $\varphi_\mu(x)$ is a linear quasi-Bloch function pertaining to chemical potential μ, and $\Phi(x,t)$ is a slowly varying amplitude, for which an averaged NLS equation can be derived as in Ref. [27],

$$i\frac{\partial\Phi}{\partial t} = -\frac{1}{2M}\frac{\partial^2\Phi}{\partial x^2} + G|\Phi|^2\Phi. \tag{5}$$

Here $M<0$ is the above-mentioned effective mass, and $G>0$ is an effective nonlinearity coefficient, which can be found by matching obvious soliton solutions to Eq. (5), $\Phi=A\,\mathrm{sech}(A\sqrt{-MG}x)$ (A is an arbitrary amplitude), to the envelope of the numerically found GSs. As a result, for the three quiescent GSs displayed in Fig. 2 we find $G=0.68$ (a), 0.41 (b), and 0.13 (c). The availability of stable moving solitons suggests to consider collisions between them. As predicted by the averaged equation (5), moving GSs emerge unscathed from collisions; see an example in Fig. 5.

The GSs displayed above are *loosely bound* solutions, in terms of Ref. [27], as they are generated by the GPE with a relatively small strength (ε) of the pinning potential. For larger ε, bands between the gaps in the model's spectrum become nearly invisible, and the character of GS solutions drastically alters, with a large variety of *tightly bound* solitons found in the broad band gaps. Figure 6(a) displays four different kinds of the solutions (for $\varepsilon=5$) with equal amplitudes, $|\phi(x=L/2)|=2$. In the first potential well around the central point, all the profiles are almost identical, but the next pair of peaks appears at markedly different positions, and may even have different signs. The form of the quasiperiodic potential $U(x)$ is displayed below the GSs. Naturally, local maxima of $|\phi|$ are found near minima of the potential. In fact, more GS species can be found, in addition to the four ones shown here. Figure 6(b) quantifies four GS families, whose representatives are displayed in Fig. 6(a), in terms of the $\mu(N)$ dependence. The curves overlap at sufficiently small N, as in this limit each GS species virtually reduces to the single peak in the first potential well; however, the species become very different at larger N, corresponding to the different GS shapes displayed in Fig. 6(a). For example, branch 4 starts to deviate from the other three ones near $N=0.5$, when negative peaks begin to develop near $x=16$ and 24.

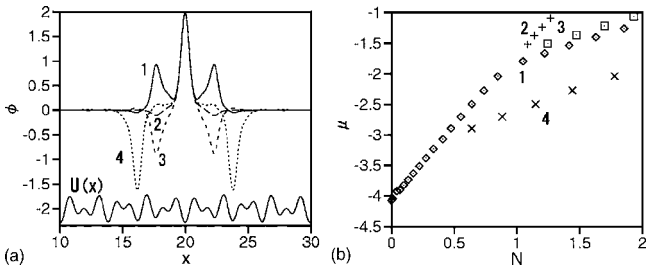

FIG. 6. (a) Four types of stationary gap solitons found in the 1D model with a strong optical lattice, $\varepsilon=5$. The chemical potential μ and the norm N are, respectively, $\mu=-1.261$, $N=1.853$ (1), $\mu=-1.088$, $N=1.266$ (2), $\mu=-1.214$, $N=1.697$ (3), and $\mu=-1.2415$, $N=2.854$ (4). The form of the potential is shown in the bottom. Panel (b) displays curves $\mu(N)$ for the four species of the gap solitons. Solution branches shown in (b) terminate at points where the solitons quickly develop the tail structures.

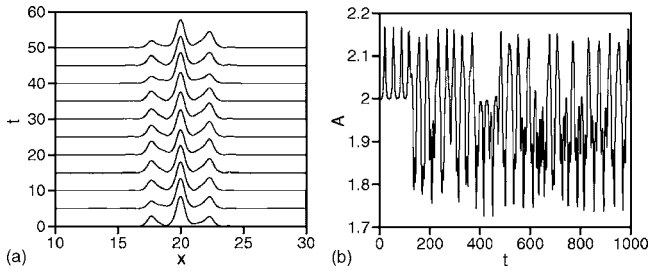

FIG. 7. (a) Evolution of $|\phi|$ for an unstable gap soliton labeled by 3 in Fig. 6(a). (b) Evolution of $|\phi(L/2)|$ in the gap soliton.

Direct simulations demonstrate that the GS species labeled as 1, 2, and 4 in Fig. 6 are *stable*, while the family labeled by 3 is *unstable*. Further, Fig. 7(a) displays a typical example of the evolution of an unstable GS. The instability breaks the soliton's symmetry and makes it a breather. Although the breathers's amplitude features complex oscillations, see Fig. 7(b), the breather does not decay, maintaining its localized shape.

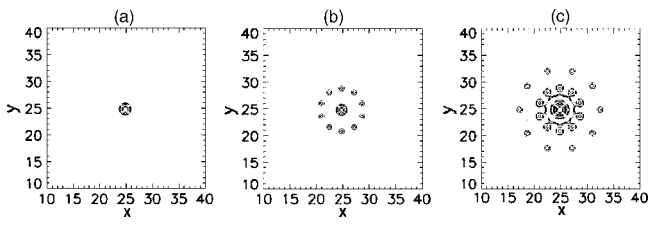

FIG. 8. Contour plots of $|\phi(x,y)|$ for three examples of stable gap solitons in the 2D model with a strong Penrose-tiling optical lattice, $\varepsilon=5$. The solitons are generated by initial conditions (8), with, respectively, $\mu=-1.56$ (a), $\mu=-3.33$ (b), and $\mu=-0.41$ (c). The norms of the three solitons are $N_a=5.61$, $N_b=3.93$, and $N_c=10.2$.

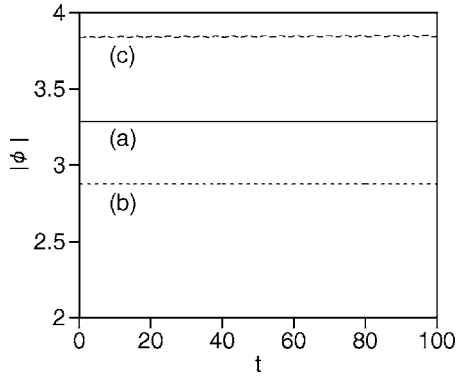

FIG. 9. Time dependence of the peak amplitudes of three localized solutions shown in Fig. 8.

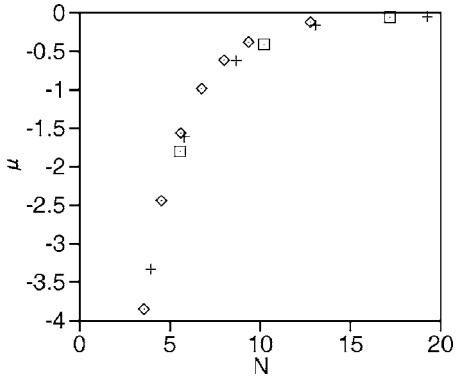

FIG. 10. Chemical potential μ of two-dimensional fundamental solitons vs N, in the model with $\varepsilon=5$. Rhombuses, crosses, and squares represent soliton families generated, respectively, by three initial configurations in Eq. (8) (typical examples of solitons belonging to the three families are given in Fig. 8).

III. TWO-DIMENSIONAL SOLITONS

In the normalized form, the 2D version of the GPE with the PT (Penrose tiling) potential is

$$i\frac{\partial\phi}{\partial t} = -\frac{1}{2}\nabla^2\phi + |\phi|^2\phi - \varepsilon\left[\sum_{n=1}^{5}\cos(\mathbf{k}^{(n)}\cdot\mathbf{r})\right]\phi, \quad (6)$$

with $\{k_x^{(n)}, k_y^{(n)}\} = \pi\{\cos[2\pi(n-1)/5], \sin[2\pi(n-1)/5]\}$. GS solutions in two dimensions were constructed by means of a combination of the known method of the integration in imaginary-time [28] and subsequent real-time simulations. To this end, a substitution was first made, $\phi(x,y,t) = e^{-i\mu t}\Phi(x,y,-i\tau)$, which transforms Eq. (6) into a nonlinear diffusion equation,

$$\frac{\partial\Phi}{\partial\tau} = \frac{1}{2}\nabla^2\Phi + (\mu_0 - \Phi^2)\Phi + \varepsilon\left[\sum_{n=1}^{5}\cos(\mathbf{k}^{(n)}\cdot\mathbf{r})\right]\Phi. \quad (7)$$

This equation was solved numerically by dint of the split-step Fourier method with 256×256 modes, in a domain of the size of 50×50. It was observed that the norm of the solution originally decreased, and then began to increase. The imaginary-time integration was switched back into simulation of the GPE in real time when the norm attained its minimum.

First, we present typical examples of stable fundamental (zero-vorticity) 2D solitons, for $\mu=-1.56$, -3.33, and -0.41. They were generated by initial conditions [in Eq. (7)] with, respectively,

$$\Phi_0(x,y) = \left\{\begin{array}{c}\exp[-0.5(x^2+y^2)]\\ 1.5\exp[-0.15(x^2+y^2)]\\ 2\exp[-0.05(x^2+y^2)]\end{array}\right\}\sum_{n=1}^{5}\cos\left(\frac{1}{2}\mathbf{k}^{(n)}\cdot\mathbf{r}\right), \quad (8)$$

the last multiplier being a half-harmonic counterpart of the PT potential in Eq. (6), which is expected to parametrically couple to the potential.

Figure 8 displays contour plots of $|\phi(x,y)|$ in final states produced by the numerical integration. To illustrate the proximity of the solutions to truly stationary ones, and their stability, in Fig. 9 we show the asymptotic time dependence of the peak amplitudes of the three solitons at $(x,y)=(L/2,L/2)=(25,25)$. These gap solitons are found in a strong optical lattice with $\varepsilon=5$, for which bands separating the spectral gaps are extremely narrow.

Systematic results for fundamental 2D solitons were generated by using initial conditions (8) and varying the respective chemical potential μ. Figure 10 shows $\mu(N)$ dependences for three families of thus generated GSs, where $N=\int\int|\phi(x,y)|^2dxdy$ is the usual 2D norm. At relatively small

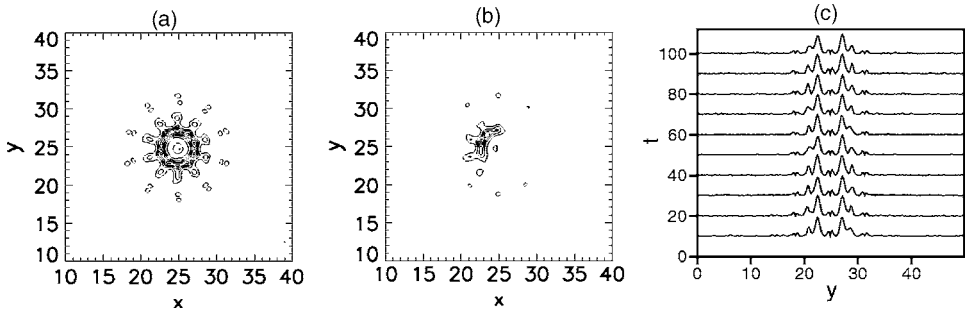

FIG. 11. A typical example of a stable vortical gap soliton with $S=-1$, found in the model with $\varepsilon=5$. (a) and (b) Contour plots of $|\phi(x,y)|$ and Re $\phi(x,y)$, the latter shown only in the region with Re $\phi(x,y)>0$. (c) A sequence of central cross sections, $|\phi(x=L/2,y)|$, taken at different moments of time, which demonstrate the vanishing of the field at the center, as must be in the vortex, and its stability. The norm and chemical potential of the solution are $N=9.69$ and $\mu=-3$.

values of N, the dependences completely overlap, and they slightly split up at very large N, corresponding to $\mu \to -0$. They are somewhat (but not quite) similar to plots for tightly bound GSs in the 1D model, cf. Fig. 6(b). There are no loosely bound stable GSs in two dimensions, because the averaged two-dimensional NLS equation [a 2D counterpart of Eq. (5)] does not have stable soliton solutions.

Lastly, stable 2D solitons with *embedded vorticity* S can be found too. They were generated by adding a factor, $(x^2+y^2)^{|S|/2}\exp(iS\theta)$, which distinguishes vortex states in uniform media, to initial *Ansätze* (8). A typical example of such a stable *vortical gap soliton* is presented in Fig. 11. While the field pattern of $|\phi(x,y)|$, displayed in Fig. 11(a), is stationary, Fig. 11(b) is actually a snapshot, as the pattern of Re $\phi(x,y)$ shown in this panel rotates clockwise, at the angular velocity of $\omega=\mu/S=-3$.

IV. CONCLUSION

We have constructed families of 1D and 2D gap solitons in the model combining the self-defocusing nonlinearity and quasiperiodic lattice potentials. Loosely bound 1D solitons supported by a weak lattice were found in three gaps; they are mobile, and collide elastically. The strong 1D lattice supports a variety of species of tightly bound solitons. Most of them are stable, unstable ones giving rise to robust asymmetric breathers. 2D gap solitons, both fundamental and vortical ones, are stable too, and they may only have a tightly bound shape. The predicted solitons can be created by means of available experimental techniques in a Bose-Einstein condensate with a positive scattering length, loading it into an optical lattice induced by a superposition of several laser beams.

ACKNOWLEDGMENTS

B.A.M. appreciates the hospitality of the Department of Applied Science for Electronics and Materials at the Interdisciplinary Graduate School of Engineering Sciences, Kyushu University (Fukuoka, Japan). This work was supported, in part, by a Grant-in-Aid for Scientific Research No. 17540358 from the Ministry of Education, Culture, Sports, Science and Technology of Japan, and the Israel Science Foundation through a Center-Excellence Grant No. 8006/03.

[1] K. E. Strecker, G. B. Partridge, A. G. Truscott, and R. G. Hulet, Nature (London) **417**, 150 (2002); L. Khaykovich, F. Schreck, G. Ferrari, T. Bourdel, J. Cubizolles, L. D. Carr, Y. Castin, and C. Salomon, Science **296**, 1290 (2002).

[2] S. L. Cornish, S. T. Thompson, and C. E. Wieman, Phys. Rev. Lett. **96**, 170401 (2006).

[3] C. J. Pethik and H. Smith, *Bose-Einstein Condensation in Dilute Gases* (Cambridge University Press, Cambridge, 2002).

[4] F. Kh. Abdullaev, B. B. Baizakov, S. A. Darmanyan, V. V. Konotop, and M. Salerno, Phys. Rev. A **64**, 043606 (2001); I. Carusotto, D. Embriaco, and G. C. La Rocca, *ibid.* **65**, 053611 (2002).

[5] B. B. Baizakov, V. V. Konotop, and M. Salerno, J. Phys. B **35**, 5105 (2002); E. A. Ostrovskaya and Yu. S. Kivshar, Phys. Rev. Lett. **90**, 160407 (2003).

[6] V. A. Brazhnyi and V. V. Konotop, Mod. Phys. Lett. B **18**, 627 (2004).

[7] K. M. Hilligsøe, M. K. Oberthaler, and K.-P. Marzlin, Phys. Rev. A **66**, 063605 (2002); D. E. Pelinovsky, A. A. Sukhorukov, and Y. S. Kivshar, Phys. Rev. E **70**, 036618 (2004).

[8] B. Eiermann, Th. Anker, M. Albiez, M. Taglieber, P. Treutlein, K.-P. Marzlin, and M. K. Oberthaler, Phys. Rev. Lett. **92**, 230401 (2004).

[9] Th. Anker, M. Albiez, R. Gati, S. Hunsmann, B. Eiermann, A. Trombettoni, and M. K. Oberthaler, Phys. Rev. Lett. **94**, 020403 (2005).

[10] T. J. Alexander, E. A. Ostrovskaya, and Y. S. Kivshar, Phys. Rev. Lett. **96**, 040401 (2005).

[11] P. G. Kevrekidis, B. A. Malomed, D. J. Frantzeskakis, A. R. Bishop, H. E. Nistazakis, and R. Carretero-Gonzalez, Math. Comput. Simul. **69**, 334 (2005).

[12] B. B. Baizakov, M. Salerno, and B. A. Malomed, in *Nonlinear Waves: Classical and Quantum Aspects*, edited by F. Kh. Abdullaev and V. V. Konotop (Kluwer Academic, Dordrecht, 2004), p. 61; also available at http://rsphy2.anu.edu.au/~asd124/Baizakov_2004_61_NonlinearWaves.pdf.

[13] H. Sakaguchi and B. A. Malomed, J. Phys. B **37**, 2225 (2004); E. A. Ostrovskaya and Y. S. Kivshar, Phys. Rev. Lett. **93**, 160405 (2004).

[14] P. Xie, Z.-Q. Zhang, and X. Zhang, Phys. Rev. E **67**, 026607 (2003); A. Ferrando, M. Zacarés, P. Fernández de Córdoba, D. Binosi, and J. A. Monsoriu, Opt. Express **11**, 452 (2003).

[15] A. Ferrando, M. Zacarés, P. Fernández de Córdoba, D. Binosi, and J. A. Monsoriu, Opt. Express **12**, 817 (2004).

[16] N. K. Efremidis, S. Sears, D. N. Christodoulides, J. W. Fleischer, and M. Segev, Phys. Rev. E **66**, 046602 (2002).

[17] J. W. Fleischer, M. Segev, N. K. Efremidis, and D. N. Christodoulides, Nature (London) **422**, 147 (2003).

[18] D. N. Neshev, T. J. Alexander, E. A. Ostrovskaya, Y. S. Kivshar, H. Martin, I. Makasyuk, and Z. Chen, Phys. Rev. Lett. **92**, 123903 (2004); J. W. Fleischer, G. Bartal, O. Cohen, O. Manela, M. Segev, J. Hudock, and D. N. Christodoulides, *ibid.* **92**, 123904 (2004).

[19] G. Bartal, O. Manela, O. Cohen, J. W. Fleischer, and M. Segev, Phys. Rev. Lett. **95**, 053904 (2005).

[20] B. B. Baizakov, M. Salerno, and B. A. Malomed, Europhys. Lett. **63**, 642 (2003); J. Yang and Z. H. Musslimani, Opt. Lett. **28**, 2094 (2003).

[21] H. Sakaguchi and B. A. Malomed, Europhys. Lett. **72**, 698 (2005).

[22] M. A. Kaliteevski, S. Brand, R. A. Abram, T. F. Krauss, R. M. De La Rue, and P. Millar, J. Mod. Opt. **47**, 1771 (2000); M. Hase, H. Miyazaki, M. Egashira, N. Shinya, K. M. Kojima, and S. I. Uchida, Phys. Rev. B **66**, 214205 (2002); M. A. Kaliteevski, S. Brand, and R. A. Abram, J. Phys.: Condens.

Matter **16**, 1269 (2004).
[23] L. M. Kahn, K. Huang, and D. L. Mills, Phys. Rev. B **39**, 12449 (1989).
[24] M. Johansson and R. Riklund, Phys. Rev. B **49**, 6587 (1994); B. Lindquist, M. Johansson, and R. Riklund, *ibid.* **50**, 9860 (1994).
[25] P. J. Y. Louis, E. A. Ostrovskaya, and Y. S. Kivshar, Phys. Rev. A **71**, 023612 (2005); M. A. Porter and P. G. Kevrekidis, SIAM J. Appl. Dyn. Syst. **4**, 783 (2005).
[26] P. Xie, Z.-Q. Zhang, and X. Zhang, Phys. Rev. E **67**, 026607 (2003).
[27] H. Sakaguchi and B. A. Malomed, J. Phys. B **37**, 1443 (2004).
[28] M. L. Chiofalo, S. Succi, and M. P. Tosi, Phys. Rev. E **62**, 7438 (2000).